REVISTA DE METALURGIA, 42 (6)
NOVIEMBRE-DICIEMBRE, 425-443, 2006
ISSN: 0034-8570

High temperature corrosion of metallic interconnects in solid oxide fuel cells*

D. M. Bastidas**

Abstract

Research and development has made it possible to use metallic interconnects in solid oxide fuel cells (SOFC) instead of ceramic materials. The use of metallic interconnects was formerly hindered by the high operating temperature, which made the interconnect degrade too much and too fast to be an efficient alternative. When the operating temperature was lowered, the use of metallic interconnects proved to be favourable since they are easier and cheaper to produce than ceramic interconnects. However, metallic interconnects continue to be degraded despite the lowered temperature, and their corrosion products contribute to electrical degradation in the fuel cell. Coatings of nickel, chromium, aluminium, zinc, manganese, yttrium or lanthanum between the interconnect and the electrodes reduce this degradation during operation.

Keywords

Solid oxide fuel cell (SOFC). Metallic interconnect and coating. High temperature corrosion. Impedance.

Corrosión a elevada temperatura de interconectores metálicos en pilas de combustible de óxido sólido

Resumen

El uso de interconectores metálicos en pilas de combustible de óxido sólido (SOFC) en sustitución de materiales cerámicos ha sido posible gracias a la investigación y desarrollo de nuevos materiales metálicos. Inicialmente, el uso de interconectores metálicos fue limitado, debido a la elevada temperatura de trabajo, ocasionando de forma rápida la degradación del material, lo que impedía que fuesen una alternativa. A medida que la temperatura de trabajo de las SOFC descendió, el uso de interconectores metálicos demostró ser una buena alternativa, dado que son más fáciles de fabricar y más baratos que los interconectores cerámicos. Sin embargo, los interconectores metálicos continúan degradándose a pesar de descender la temperatura a la que operan las SOFC y, asimismo, los productos de corrosión favorecen las pérdidas eléctricas de la pila de combustible. Recubrimientos de níquel, cromo, aluminio, zinc, manganeso, itrio y lantano entre el interconector y los electrodos reduce dichas pérdidas eléctricas.

Palabras clave

Pilas de combustible de óxido sólido (SOFC). Interconectores metálicos y recubrimientos. Corrosión a elevada temperatura. Impedancia.

1. INTRODUCTION

Fuel cells offer a new and clean energy alternative to less efficient carbon-based and nuclear systems, for everything from transport, electricity for homes and offices, to power for laptops and mobile phones. Table I shows the five types of fuel cells used. Solid oxide fuel cells (SOFC) are competing on the world stage in the stationary energy market, for portable applications, and for residential combined heat and power

* Trabajo recibido el día 18 de septiembre de 2006 y aceptado en su forma final el día 9 de octubre de 2006.
** CENIM-National Centre for Metallurgical Research, CSIC, Avda. Gregorio del Amo 8, 28040 Madrid, Spain, E-mail: david.bastidas@cenim.csic.es

Table I. Summary of fuel cell types. AFC: alkaline fuel cell, SPFC: solid polymer proton conductor fuel cell, PAFC: phosphoric acid fuel cell, MCFC: molten carbonate fuel cell, and SOFC: solid oxide fuel cell

Tabla I. Resumen de los tipos de pilas de combustible. AFC: pilas de combustible alcalinas, SPFC: pilas de combustible de polímeros sólidos conductores de protones, PAFC: pilas de combustible de ácido fosfórico, MCFC: pilas de combustible de carbonatos fundidos, y SOFC: pilas de combustible de óxido sólido

Description	Fuel cell					
	AFC	AFC	SPFC	PAFC	MCFC	SOFC
Anode	80 %Pt-20 %Pd	Ni	Pt black or Pt/C	Pt/C	Ni-10 % Cr	Ni-YSZ
Cathode	90 %Au-10 %Pt	Li-doped NiO	Pt black or Pt/C	Pt/C	Li-doped NiO	Sr-doped $LaMnO_3$
Electrolyte	35-40 %KOH	85 % KOH	Nafion (Du Pont)	H_3PO_4	62 %Li_2CO_3 + 38 % K_2CO_3	YSZ
Fuel	Highly pure H_2	Highly pure H_2	Pure H_2	CO-free H_2	H_2, CH_4, CO	H_2, CH_4, CO
Charge carrier	OH^-	OH^-	H^+	H^+	CO_3^{2-}	O^{2-}
Operation temperature	80-90 °C	260 °C	80-260 °C	200 °C	650 °C	800-1000 °C
Electrical efficiency	40 %	40 %	40 %	40 %	60 %	60-70 %

(CHP) generator units. This heralds a new worldwide environmentally-friendly energy appliance for energy markets where the Kyoto Agreement, in force since 2005, the need to cut CO_2 emissions by 60 % by 2050, with demonstrated progress by 2020, electricity prices, and fuel volatility are significant drives for such systems.

Global warming and the constant increase in energy demand makes it necessary to use new clean and environmentally-friendly energies. In this respect, SOFC represents one of the most promising energy sources. Environmental pollution caused by the burning of fossil fuels all over the world is a major problem to be solved.

The aim of this paper is to review the bibliography in this area and describe recent developments in SOFCs that demonstrate the use of interconnects and the applicability of the electrochemical impedance spectroscopy (EIS) method. The requirements of interconnect metallic materials, the characteristics of the leading candidate materials, the corrosion resistance and hence the lifetime they offer and how well they fulfil the requirements, and the oxidation resistance, scale properties and microstructure of chromium-containing alloy/cathode interfaces will also be described.

2. OPERATING PRINCIPLE OF A SOLID OXIDE FUEL CELL

A fuel cell consists of two sintered, porous electrodes separated by an ion-conducting electrolyte like yttria (Y_2O_3)-stabilised zirconia (ZrO_2) (YSZ). The fuel cell can operate as long as it is continuously fed with reactants and the reaction products are removed. Because it is easy to make the reactant tanks larger, a fuel cell's period of operation can be made much longer than a conventional electrochemical battery.

Fuel cell power sources are conventionally said to be non-Carnot-limited, and therefore are more efficient than heat engines. The efficiency (η_{hl}), about a maximum of 40-50 %, of a heat engine working in such a Carnot cycle between the temperatures T_1 and T_2 is the ratio of the work done during the cycle to the heat 'put in' [1]:

$$\eta_{hl} = - \frac{T_2}{T_1} \quad (1)$$

The overall fuel cell efficiency (η_{fc}) is given by:

$$\eta_{fc} = \eta_g \eta_v m \quad (2)$$

where η_g is the Gibbs efficiency:

$$\eta_g = \frac{\Delta G}{\Delta H} = \frac{nFE_{0CV}}{\Delta H} \quad (3)$$

ΔH is the heat of the overall cell reaction; η_v is the voltage (E) efficiency:

$$\eta_v = \frac{E}{E_{0CV}} = \frac{E_{0CV} - I\,(ASR)}{E_{0CV}} \quad (4)$$

E_{0CV} is the open circuit voltage, and ASR is the combined area-specific resistance of the cell components (electrolyte, anode and cathode), which should ideally be 0.1 Ω cm^2; and m is the fraction of fuel used. Thus,

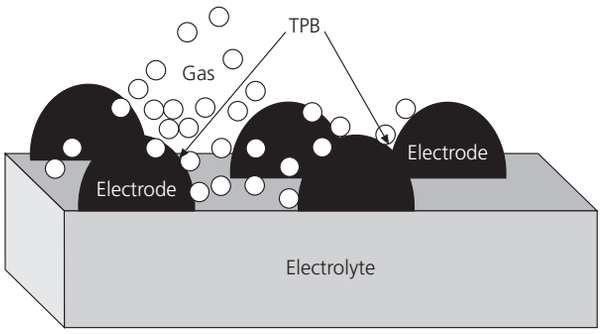

Figure 1. Triple-phase boundary (TPB) model.

Figura 1. Modelo de la triple fase (TPB).

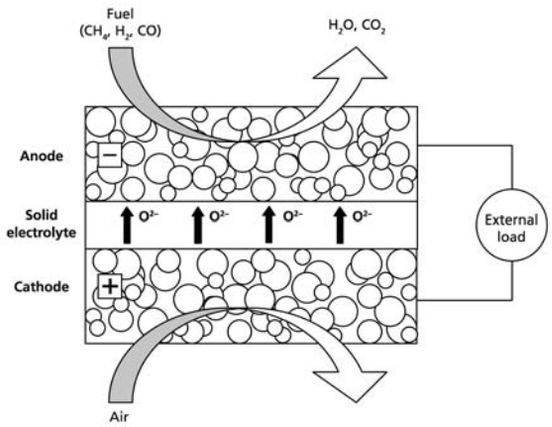

Figure 2. Diagram showing the operating principles of an SOFC.

Figura 2. Diagrama mostrando los principios de operación de un SOFC.

$$\eta_{fc} = \frac{nf\,[E_{0CV} - I\,(ASR)]m}{\Delta H} \qquad (5)$$

and the need to minimise cell resistivities has a major impact on the selection and processing of the cell components[2].

SOFC manufacturing involves the deposition of thin particulate films on substrate electrodes, followed by co-firing. A SOFC unit is formed by: (i) the cathode, frequently using strontium-doped lanthanum manganite ($LaMnO_3$), $La_xSr_{1-x}MnO_3$ (LSM), the coefficient of thermal expansion (CTE) of LSM being ~12×10^{-6} K^{-1}, $La_xSr_{x-1}Co_yFe_{1-y}O_3$ (LSCF), or the recently reported $LaNi_{0.6}Fe_{0.4}O_3$ (LNF)[3], and $Ba_xSr_{1-x}Co_yFe_{1-y}O_3$ (BSCF)[4]; (ii) the electrolyte (YSZ, doped ceria, etc.), for which YSZ exhibits good CTE (~11×10^{-6} K^{-1}) and chemical stability, high oxide-ion conductivity (~0.1 S cm^{-1} at 1000 ºC) and mechanical strength at high temperature; and (iii) the anode, usually an Ni-YSZ or an NiO-YSZ, i.e. a metallic-ceramic composite, referred as a 'cermet'. Cermets display excellent catalytic properties for breaking hydrogen bonds and good current collection but also exhibit certain disadvantages, such as low tolerance to sulphur and carbon deposition when using hydrocarbon fuels and poor redox cycling causing volume instability[5-7]. The high thermal expansion of nickel compared to YSZ is another disadvantage.

The selection of LSM cathode and Ni-YSZ anode compositions was established during the 1970s after examining a variety of oxide compositions for long-term compatibility with YSZ at elevated temperatures. This empirical conclusion was later explained in terms of available thermodynamical data[2].

Carbon deposition covers the active sites of the anodes, resulting in the loss of cell performance[8]. In high carbon activity environments iron, nickel, cobalt and alloys based on these metals could corrode by a process known as metal dusting. Metal dusting involves the disintegration of bulk metals and alloys into metal particles at high temperatures (300-850 ºC) in environments that are supersaturated with carbon. The Ni corrosion process depends strongly on the temperature and the gas composition and in general the Ni corrosion rate increases with temperature[9]. It is generally accepted that the electrochemical activity of Ni anodes for H_2 oxidation reaction depends strongly on the three-phase boundary (TPB), gas/electrode/electrolyte, e.g. where the fuel gas, Ni and YSZ phases meet (see Fig. 1)[10 and 11].

The presence of sulphur (primarily in the form of H_2S) in the fuel gas can also affect the performance of Ni-YSZ cermet anodes. The electrode polarisation resistance (Ω cm^2) increases by a factor of two by adding only 5 ppm of H_2S at 950 ºC in 97 %H_2/3 %H_2O system[8]. The poisoning effect of sulphur-containing fuel gas on electrode performance depends on the total sulphur content and the temperature[12].

SOFC is an all solid device that directly converts the chemical energy of gaseous fuels such as hydrogen and natural gas to electrical energy by means of very high efficiency electrochemical processes (~70%). They typically consist of a dense electrolyte medium sandwiched between two porous electrodes called the anode (negative electrode) and cathode (positive electrode). The anode/electrolyte/cathode sandwich is referred to as a single cell. The cathode process (the air electrode) in a SOFC normally involves the reduction of molecular oxygen to oxygen anions ($2O^{2-}$) using electrons external to the cell:

$$O_2 + 4e^- \rightarrow 2O^{2-} \qquad (6)$$

In order to accomplish this reaction the cathode should be able to dissociate O_2 and be electronically

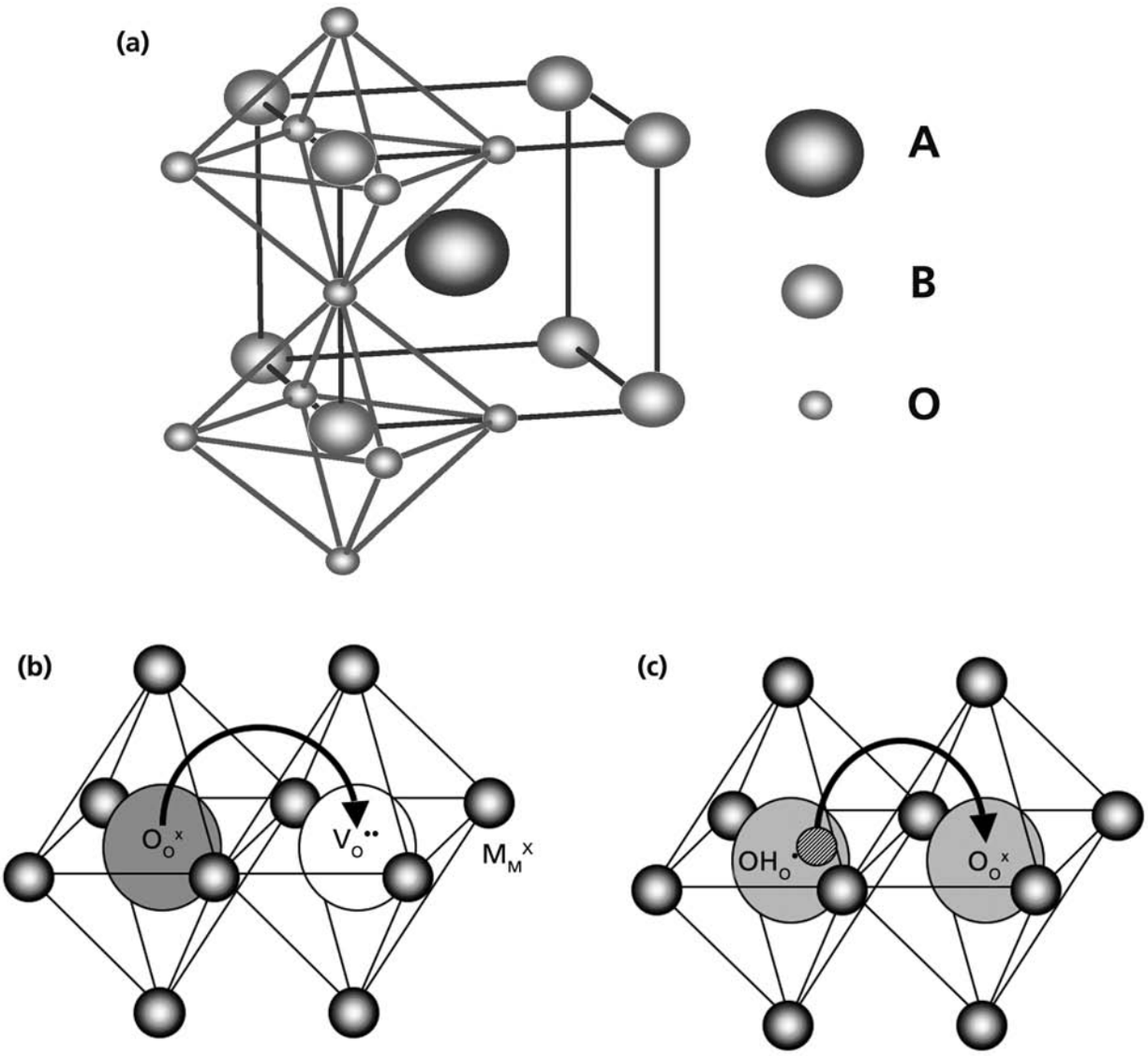

Figure 3. (a) Crystallographic structure of the perovskite ABO_3 type compound; (b) oxygen ion transport, (c) proton transport high temperature ion-conducting ceramics.

Figura 3. (a) Estructura cristalográfica de un compuesto ABO_3 tipo perovskita; (b) transporte del ion oxígeno, (c) transporte del protón a elevada temperatura en cerámicos conductores iónicos.

conductive. The oxygen anions formed are transported through the ionically conducting (but electronically insulating) solid electrolyte to the anode where they react electrochemically with the fuel gas (CH_4, H_2, CO, etc.):

$$H_2 + O^{2-} \rightarrow H_2O + 2e^- \qquad (7)$$

if H_2 is used as fuel, to generate an electrical voltage. The latter reaction can be written following Kröger-Vink notation as:

$$H_2 + O^{2-}_{YSZ} \rightarrow H_2O + 2e' + O_{\ddot{O},\,YSZ} \qquad (8)$$

where O^{2-}_{YSZ} is an oxygen ion in the YSZ electrolyte lattice site and $O_{\ddot{O},\,YSZ}$ is an oxygen vacancy in YSZ. It should be noted that the majority of H_2 is generated by reforming hydrocarbons[13]. The overall cell process is:

$$2H_2 + O_2 \rightarrow 2H_2O \qquad (9)$$

figure 2 is a schematic diagram showing how SOFCs work.

The primary advantages of fuel cells are that they provide continuous power (as long as fuel and oxidiser are supplied), have a low weight with a high output power, and an efficiency of about 70%. These

advantages make them very useful for manned missions. The main disadvantages of fuel cells are their expense and the possibility that a loss of cooling can result in an explosion. Consequently, elaborate control systems are required to keep them operating.

In any event, as long as hydrogen and oxygen are continuously fed to the fuel cell, the flow of electric current will be sustained. To meet the requirements of the application, 'interconnect' material is used to connect single cells together in series or parallel to achieve high output voltage, current and power performance. Thus it is possible to form a fuel cell stack of any desired voltage or current. The number of fuel cells in the stack determines the total voltage, and the surface area of each cell determines the total current. Multiplying the voltage (V) by the current density (A cm^{-2}) will yield the total electrical power density (W cm^{-2}) generated.

The interconnect is the means by which electronic connection is achieved between two neighbouring fuel cells. It physically separates the fuel cell, in the anode cavity, from the air or oxygen, in the cathode cavity, and at the same time helps to maintain the structural integrity of the SOFC stack. The interconnect material is conventionally made of ceramic materials, such as lanthanum chromite ($LaCrO_3$) doped with either CaO or SrO, or $La_xSr_{(1-x)}CrO_3$ (LSC), a typical high temperature ceramic interconnect material[7 and 14-16]. The recent development of sintering procedures below 1000 ºC, which should allow the use of metal substrates, represent a significant advance that will enable the development of more rugged SOFC systems. The importance of the interconnect materials relies on their electrical conductivity, and more than 70 % of the electrical losses in a SOFC system are due to the interconnect design. The high cost of raw materials and manufacturing, difficulties in obtaining high density lanthanum chromite parts, the tendency of chromite to be reduced at the fuel gas/interconnect interface, and the recent trend in developing lower temperature operation (700-850 ºC) using new electrolytes with improved conductivity, make it feasible for $LaCrO_3$ to be replaced by metals or alloys as the interconnect materials.

3. HIGH TEMPERATURE ION-CONDUCTING CERAMIC

SOFCs are based on the concept of high temperature ion-conducting ceramics. These ceramics are metal oxides typically with a perovskite or fluorite crystal structure (see Fig. 3a). In oxygen-ion conductors an oxygen ion moves from a filled (O_O^x) to a vacant oxygen site ($V_O^{\bullet\bullet}$) through a fixed cation lattice (M_M^x), as shown in figure 3b:

$$O_2 + 2V_O^{\bullet\bullet} + 4e^- \Leftrightarrow 2\,O_O^x \qquad (10)$$

Therefore, the actual charged solid-state ionic species involved in oxygen-ion transport is $V_O^{\bullet\bullet}$. In proton-conducting oxides the proton is associated with an oxygen site ($OH_O^{\bullet}$) and hops between adjacent oxygen sites, as shown in figure 3c. The effects of hydrogen or protons on the oxidation mechanisms of metals or alloys have been discussed in the literature[17]. It has been concluded that protons at the metal/oxide interface or in the oxide scales are commonly bonded to oxygen ions, forming substitutional hydroxide point defects:

$$H + O_O^x \Leftrightarrow OH_O^{\bullet} + e^- \qquad (11)$$

Because oxygen and hydrogen are transported through lattices sites the gas separation selectivity is infinite.

The ideal cathode material has good electronic and ionic conductivities and a CTE which matches that of the electrolyte. The electrolyte should be dense in order to separate the air and fuel compartments, possess high ionic conductivity, be an electronic insulator, and maintain these properties over a wide range of partial oxygen pressure (pO_2) from ~1 atm at the cathode to ~10^{-20} atm or less at the anode. The anode or fuel electrode catalyses the reaction of the fuel with oxygen anions from the electrolyte and conducts the electrons that are produced in this reaction to the external circuit.

4. SOLID OXIDE FUEL CELL CONFIGURATIONS

There are two basic SOFC configurations, planar and tubular, yielding five types of design: tubular-design, developed initially by Westinghouse, USA; Hexis-design, developed initially by Sulzer-Innotec, Switzerland; planar-design, developed initially by Siemens, Germany; flat tubular design, developed initially by Rolls Royce, UK; and micro-tubular design, developed by Acumentrics, USA and University of Birmingham, UK[18-20]. Recently a new concept is being launched: the SOFCroll, which is based upon a hybrid of the planar and tubular configurations.

4.1. Tubular configuration

Each tube is manufactured like a large test-tube, sealed at one end. Fuel flows along the outside of the tube towards the open end. Air is fed through a thin alumina air supply tube located centrally inside each tubular fuel cell (see Fig. 4). Heat generated within

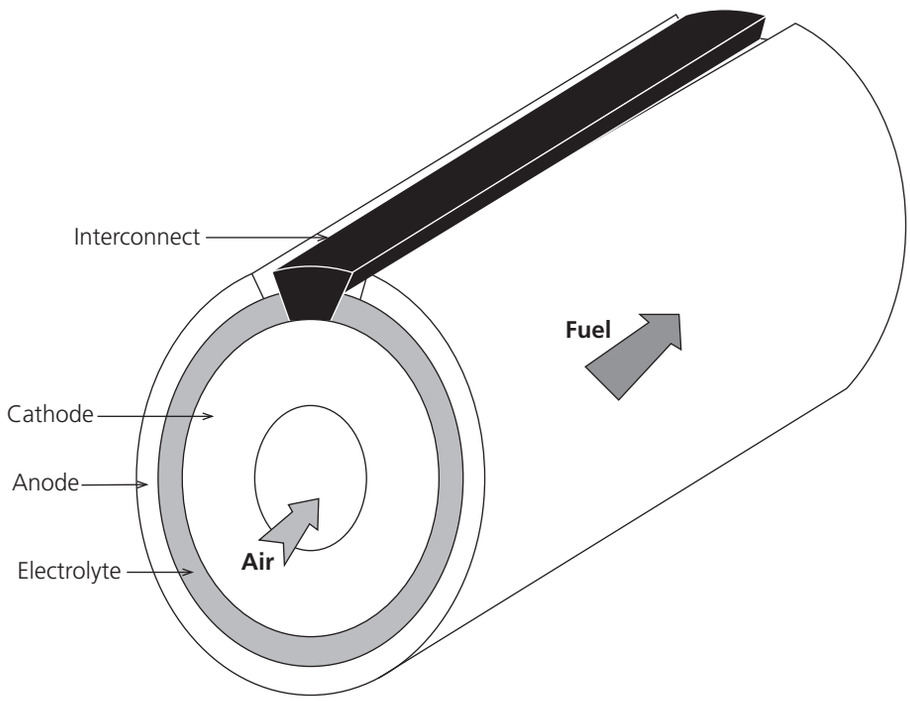

Figure 4. Tubular fuel cell design.

Figura 4. Diseño de una pila de combustible tubular.

the cell brings the air up to the operating temperature. The air then flows through the fuel cell back up to the open end. One great advantage of the tubular SOFC design is that high temperature gas-tight seals are eliminated.

4.2. Planar configuration

The planar configuration more closely resembles a type of architecture where the bipolar or flat plate structure enables a simple electrical connection in series between cells without the long current path through the tubular cell shown in figure 5. The bipolar flat plate design thus results in lower ohmic losses than the tubular arrangement (see Fig. 5), leading to superior performance and a much higher power density. Another advantage of the planar design is that low-cost manufacturing methods such as screen-printing and tape casting can be used.

An alternative to tubular and planar configurations is the new SOFCroll design (see Fig. 6)[5, 14, 15 and 21]. Tape casting, cheap and easily scalable, is utilised as the production technique, and co-firing as a single unit further reduces the cost and time of cell production. The SOFCroll geometry eliminates the need for thicker support components, resulting in higher power densities and small space requirements.

The most severe challenge for planar SOFC stacks is the poor lifetime of the CTE matching ferritic stainless steels (FSS) that are being used as interconnects and the requirement for sealants, mostly based on glass ceramics[18]. The advantages of the lower operating temperatures of SOFC stacks, 700 ºC or even 500 ºC, allows the use of FSS in cell stack construction, greatly reducing the cost. At the same time, these temperatures are not so low as to eliminate the advantages of SOFC technologies. The primary challenges when lowering the temperature are ohmic loss reduction, electrolyte stability, and cathode polarisation. The conductivity of the solid electrolyte is strongly dependent on the temperature. Acceptable conductance of the separator can be achieved by using thinner films or doping to increase conductivity[22].

Compared to ceramic materials, mostly compounds based on doped lanthanum-chromite ($LaCrO_3$), metallic materials have the following advantages: (i) the mechanical properties, strength and workability of metals are generally much better than ceramics; (ii) compared with lanthanum, an expensive rare-earth element, nickel, iron, cobalt and chromium elements are substantially cheaper; (iii) the electrical conductivity of metals is about three orders of magnitude higher than doped $LaCrO_3$; and (iv) the heat conductivity of metals is typically much higher than doped $LaCrO_3$. Improved heat conductivity will reduce stresses originated by temperature gradients in the fuel cell

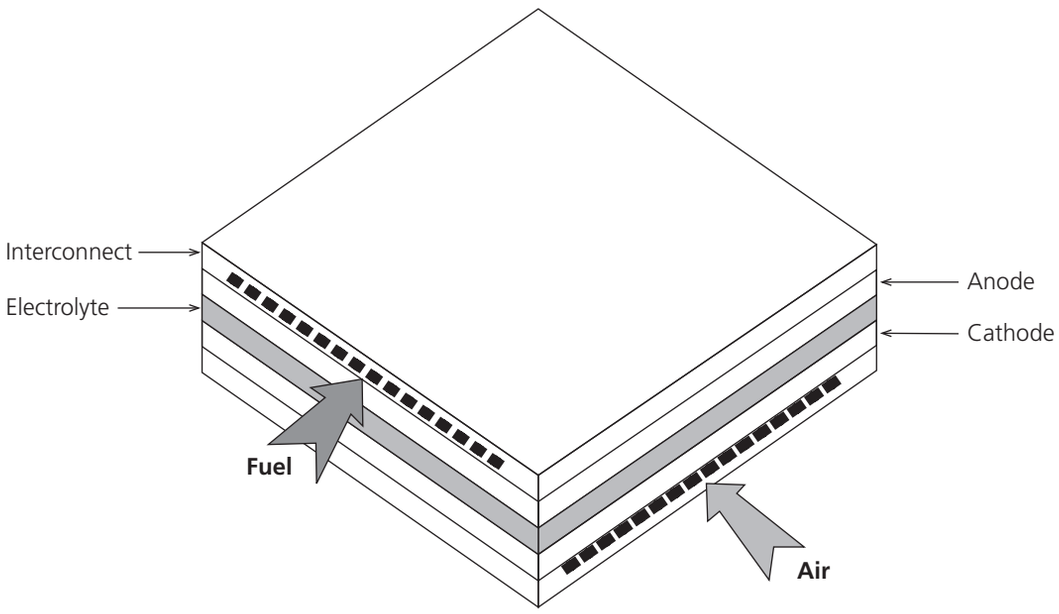

Figure 5. Planar fuel cell design.

Figura 5. Diseño de una pila de combustible plana.

stack and reduce the demand for cooling by excess gas. For systems operating at lower temperatures, 700-850 ºC, it is conceivable that metallic alloys like ferritic SS could be used. Other chromium-base superalloys have also been tested[23]. The major difficulty with such ceramic interconnects is the difficulty of sintering to full density. Lanthanum chromite ($LaCrO_3$) powders do not sinter easily, especially in oxidising atmospheres.

Based on the requirements of oxidation resistance, low CTE and the electrical conductivity of surface oxide scales, chromium-base alloys and high-chromium ferritic SSs seem to be the most promising metallic interconnect materials. Whereas chromium-base alloys have recently been specially developed for SOFC application, a large number of ferritic SSs are commercially available in a wide range of compositions. However, it seems that the specific combination

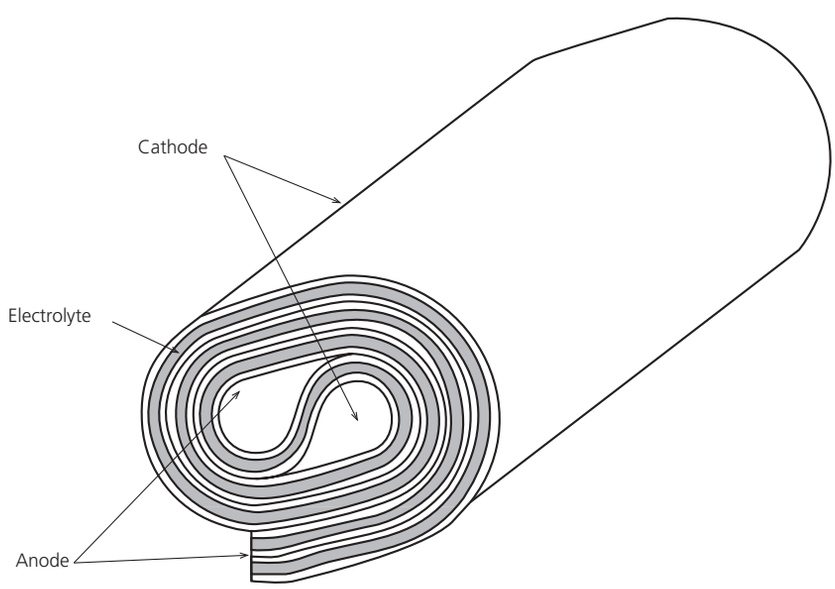

Figure 6. SOFCroll design (curled fuel cell geometry).

Figura 6. Diseño SOFCroll (pila de combustible con geometría curvada).

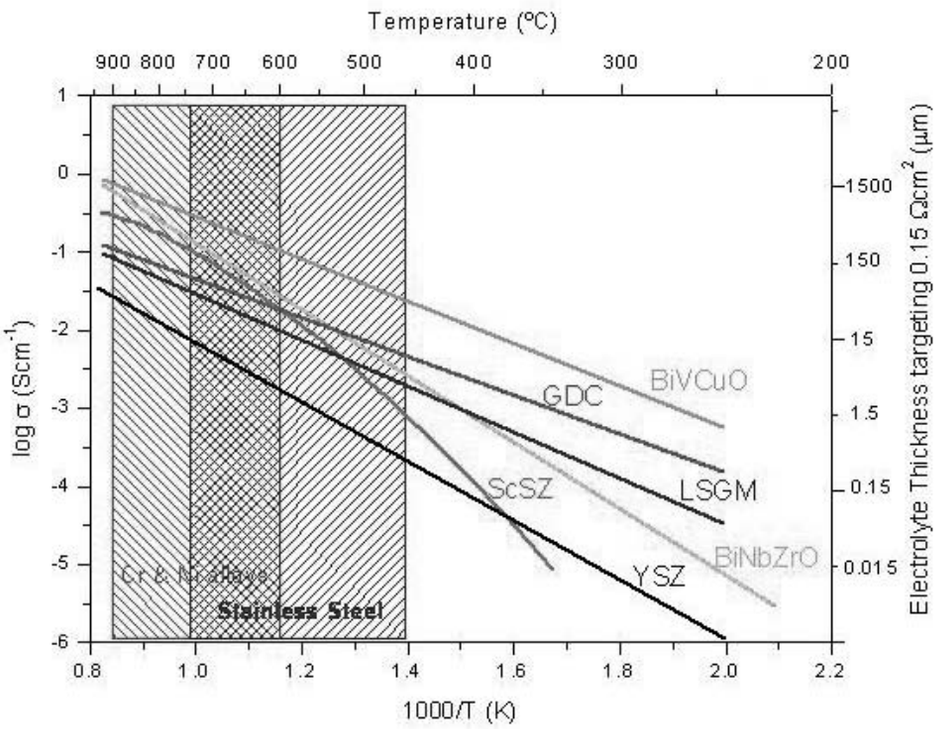

Figure 7. Specific conductivity versus reciprocal temperature for selected solid-oxide electrolytes.

Figura 7. Conductividad específica frente al reciproco de la temperatura de electrólitos de óxido sólido.

of properties required by SOFC interconnects will necessitate the development of a new, specifically designed steel or the modification of an existing commercial steel composition.

Other challenges are related with the likely presence of water vapour in both anodic (fuel) and cathodic (air) environments and the possibility of the fuel containing sulphide impurities. The interconnect should also be stable toward any sealing materials it may be in contact with.

To avoid these problems, metal interconnects are being used. The alloy is largely chromium with 5 wt. % iron and 1 wt. % yttria to give dispersion strengthening. This alloy has almost the same CTE as YSZ and has the benefit of improved strength and toughness compared with lanthanum chromite. However, it requires coating to prevent chromium migration and is also an expensive option at the present time[7].

If it is assumed that the electrolyte component should not contribute more than 0.15 Ω cm^2 to the total cell ASR (area-specific-resistance), then for a thick-film thickness (ξ) of 15 μm, the associated specific ionic conductivity (σ) of the electrolyte should exceed 10^{-2} S cm^{-1} ($\sigma = \xi/ASR = 0.0015cm/0.15\Omega cm^2$), (see Fig. 7).

The advantages of metallic interconnects over ceramic interconnects include lower material and manufacturing costs, the possibility of easier and more complex shaping, better electrical and thermal conductivity and no deformation or failure due to different gas atmospheres across the interconnection. Interconnects can be manufactured by machining, pressing, or, in the case of powder metallurgical alloys, by near-net-shape sintering. The gas distribution is usually achieved by parallel channels, with the ridges that separate the channels serving as electrical contact with the electrodes.

It is generally accepted that the oxidation of stainless steels (SS) and nickel-base alloy materials is one of the most serious disadvantages for their application in SOFCs[16]. At low temperatures, pitting corrosion of SS is the main limitation for industrial applications[24-27].

5. COMPOSITION CRITERIA FOR INTERCONNECT SELECTION

In terms of chemical composition, high-temperature corrosion resistant alloys may be classified as (a) Ni-, Fe- and Co-base superalloys, (b) Cr-base alloys, and (c) Fe-C base alloys containing chromium, i.e. stainless steels (SS). All of these alloys typically contain chromium and/or aluminium (silicon is a third possibility, but much less used) to provide oxidation resistance by forming oxide scales of chromia (Cr_2O_3) and alumina (Al_2O_3), respectively.

5.1. Nickel- and iron-base superalloys

In Ni- and Fe-base superalloys the critical minimum chromium content necessary to ensure the formation of a protective, continuous Cr_2O_3 scale is approximately 20-25% chromium. However there are few appropriate superalloys with a chromium content of more than 18 wt. % and an aluminium content of more than 3%. For cobalt-base superalloys an optimum content of 25-30% chromium for hot corrosion has been indicated. On the other hand, conventional Co-base alloys do not contain aluminium[28].

5.2. Chromium-base alloys

Chromium-base alloys crystallise in the body-centred-cubic (bcc) structure and are not considered as superalloys. Aluminium is not included in these compositions. Another challenge for metallic SOFC interconnects is the evaporation of chromium species from the protective Cr_2O_3 layer and the poisoning effects of these species at the electrode/electrolyte interfaces[29]. Chromium-base alloys have been researched in detail with regard to corrosion behaviour and contact resistance across their interfaces with the electrodes. Thicker corrosion scales grow in carbon-containing atmospheres (methane, propane, liquefied petroleum gas (LPG), coal gas) due to the formation of carbides.

The manufacturing of $Cr_5FeY_2O_3$ interconnect plates is achieved by powder metallurgy methods and starts with the alloying of chromium flakes with iron and yttria (Y_2O_3) by high-energy milling. Pressing and sintering in a hydrogen atmosphere is followed by a hot forming process such as hot rolling in a vacuum. For this purpose, however, new materials need to be developed with different chromium powder grades, additional alloying elements, and different oxide dispersoids to improve sinterability, pressing behaviour, resulting density, corrosion and contact resistance with thermally sprayed protective coatings. These coatings are necessary, on the one hand, to improve the contact between the interconnect and the adjacent electrode and, on the other hand, to prevent fast deterioration of cell performance. A stack endurance test with one of these near-net-shape alloys showed very stable performance for a period of 1000 h [28].

5.3. Stainless steels (SS)

These are Fe-C base alloys and contain chromium. They are commonly used because of their pitting corrosion resistance[30]. Depending on their crystal and microstructures, SSs are: (1) austenitic SSs; (2) ferritic SSs; (3) duplex SSs (austenitic-ferritic), in which the ratio of ferrite to austenite depends mainly on the nickel content (~4.5-8 %), presenting a CTE for 2205 of 14×10^{-6} K^{-1} and 13×10^{-6} K^{-1} for SAF 2304; (4) martensitic SSs; and (5) precipitation-hardening SSs. With regard to ferritic SSs, a minimum of 13 % chromium is required to maintain the body-centred-cubic (bcc) ferritic structure, and therefore they are not susceptible to strengthening by heat-treatment. In contrast to chromium, the interstitial elements carbon and nitrogen are austenite formers, characterised by the γ austenitic face-centred-cubic (fcc) matrix, and thus their concentrations are preferably controlled at a low level in ferritic structures.

Like iron-base superalloys, a critical minimum chromium content of 18% and a critical maximum aluminium content of 3% are recommended for Fe-base SSs. It has been reported that for planar SOFCs with service temperatures of 700-850 ºC the stainless steel's chromium content should be higher than ~17%[31]. Considering the possible depletion of chromium through interaction with contact materials, the chromium content in SS should be higher than ~22%[28]. According to these composition criteria (Cr_2O_3 and Al_2O_3 forming), martensitic and precipitation-hardening grades were excluded from consideration. Also,

Table II. Properties of some alloy groups for SOFC applications, from room temperature to 800 °C. Matrix structures are (bcc) body-centred-cubic, and (fcc) face-centred-cubic

Tabla II. Propiedades de algunos grupos de aleaciones para ser aplicados en SOFC, de temperatura ambiente a 800 ºC. La estructura de la matriz es (bcc) cúbica centrada en el cuerpo, y (fcc) cúbica centrada en las caras

Material	Matrix Structure	CTE $\times10^{-6}$ K^{-1}	Oxidation resistance	Mechanical strength
Cr-base alloys (CrBA)	bcc	11.0-12.5	Good	High
Ferritic stainless steels (FSS)	bcc	10.5-14.0	Good	Low
Austenitic stainless steels (ASS)	fcc	16.2-20.0	Good	High
Fe-Ni-base superalloys (FeBSA)	fcc	15.0-20.0	Good	High
Ni-Fe-base superalloys (NiBSA)	fcc	14.0-19.0	Good	High

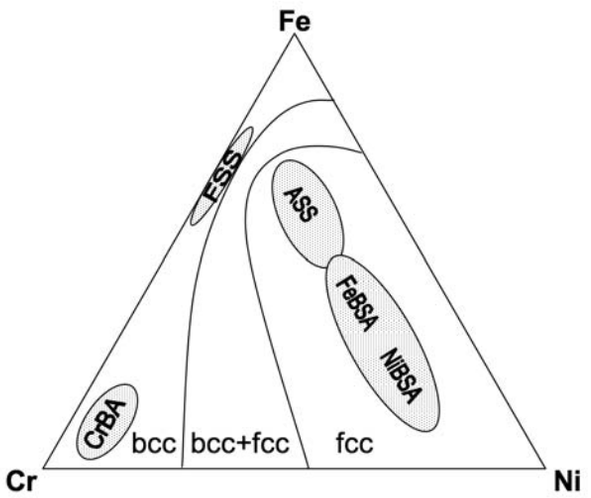

Figure 8. Fe-Ni-Cr phase diagram for SOFC applications, bcc (body-centred-cubic) and fcc (face-centred-cubic). CrBA: Cr-base alloys, FSS: ferritic stainless steels, ASS: austenitic stainless steels, FeBSA: Fe-Ni-base superalloys, and NiBSA: Ni-Fe-base superalloys.

Figura 8. Diagrama de fases de Fe-Ni-Cr para aplicación en SOFC, bcc (cubico centrado en el cuerpo) y fcc (cúbico centrado en las caras). CrBA: aleaciones base cromo, FSS: aceros inoxidables ferríticos, ASS: aceros inoxidables austeniticos, FeBSA: superaleaciones base Fe-Ni, y NiBSA: superaleaciones base Ni-Fe.

the high coefficient of thermal expansions (CTE) of austenitic SS makes it difficult to find applications for them. Figure 8 shows a Fe-Ni-Cr phase diagram for all the groups of alloys, excluding the cobalt-base alloys. Table II indicates the structural characteristics and properties of the different alloys of figure 8.

5.4. Ferritic stainless steels

Compared with $Cr_5FeY_2O_3$, ferritic stainless steels have the advantages of the lower cost of the material, easier processing and manufacturing of components, weldability, and thermal expansion match with the anode substrate, 10.5×10^{-6} K^{-1} for AISI 430 and $\sim12\times10^{-6}$ K^{-1} for Crofer22 APU and AL 453. When using CrAl18 the growth of nodular corrosion products led to partial delamination of the cathode contact layer from the cathode. Therefore it became evident that new steel compositions with better corrosion resistance than commercially available ferritic stainless steels needed to be developed.

The CTE of ferritic stainless steels decreases as the chromium content is raised up to 20 wt. % and increases as the aluminium content is raised. By such alloying the thermal expansion of ferritic stainless steels can be adjusted and matched to the Ni-YSZ cermet anode substrate, but not to the YSZ electrolyte. The oxidation of stainless steels depends not only on the chromium content but also on the small amounts of alloying elements, especially aluminium and silicon. Once a compositional threshold is reached, alumina and silica layers are formed instead of a chromia layer. This leads to a reduction in the oxidation rate. However, these alumina and silica layers are insulating and need to be avoided when the stainless steel interconnect is in contact with a contact or electrode material.

Other studies have investigated powder metallurgy model steels containing 22-26 % chromium and minor additions of molybdenum, titanium, niobium and Y_2O_3. After oxidation in air, all the materials showed a double-layered oxide scale composed of chromia directly in contact with the alloy and manganese-chromium spinel at the outer surface.

However, the corrosion behaviour of thin foils of ferritic stainless steels can be very different compared to that of thick plates, due to the effect of selective oxidation and depletion of alloyed elements leading to composition changes in the foil. As long as the metallic component is thick enough to serve as a quasi-infinite chromium reservoir, chromium enrichment at the surface (i.e. the formation of chromia scale) has no significant influence on the composition of the thick steel plate. Nevertheless, when thin foils are used, the amount of chromium is limited and chromia formation can give rise to compositional changes within the thin foil, leading to very different corrosion behaviour. Tests over several thousand hours are required to demonstrate the reliability of these lightweight interconnect designs.

6. EVALUATION OF INTERCONNECT PROPERTIES FOR SOFC APPLICATIONS

New trends in advanced materials research and development are being pursued in an attempt to reduce high-temperature corrosion: development in understanding of high-temperature corrosion and protection in aggressive environments; high-temperature coatings (including thermal barrier coatings); high-temperature alloys and intermetallics; ceramics and composites; metal dusting and carburisation; role of water vapour and steam in high-temperature corrosion; modelling and lifetime prediction; spalling and mechanical aspects; and advanced characterisation techniques of degradation.

The requirements for a metal to be used as an interconnect material are rather extensive and somewhat dependent upon the particular SOFC configuration[2, 13, 32 and 33]. Some of these requirements are:

(1) The coefficient of thermal expansion (CTE) should be close to that of the cell elements, namely the cathode, strontium-doped $LaMnO_3$ (LSM), and particularly the electrolyte (YSZ), i.e. around ~11×10^{-6} K^{-1} in the temperature range between the operating temperature and room temperature.

(2) The metal should show good resistance to high-temperature corrosion, e.g. oxidation, carburisation and nitriding.

(3) The oxide layers formed on the metal surface should present good adhesion to the metal and the electrical resistivity of both the oxide layer and the metal/oxide scale should be low.

(4) The metal should be gas-tight and its permeability to protons (H^+) and oxygen anions (O^2) should be low.

(5) Reactions between the alloy and oxide scale and the electrodes should not diminish the cell's properties. Unwanted reactions include evaporation of oxide, e.g. CrO_3 vapour released from the Cr_2O_3 oxide layer. When Cr_2O_3(s) is exposed in dry air at temperatures higher than approximately 873 K, CrO_3 vapour is easily produced from the surface of Cr_2O_3(s) by the reaction:

$$1/2Cr_2O_3(s) + 3/4O_2(g) \Leftrightarrow CrO_3(g) \qquad (12)$$

Furthermore, the presence of a small amount of water vapour in air significantly increases the vapour pressure of Cr species by the reaction:

$$1/2Cr_2O_3(s) + 3/4O_2(g) + H_2O(g) \Leftrightarrow CrO_2(OH)_2(g) \qquad (13)$$

from the catalytic active surfaces of the electrodes[3 and 34].

(6) The price of the alloy in the final form should be sufficiently low to make the SOFC technology commercially feasible.

Of the requirements listed above, the first three are crucial and tend to eliminate most candidate materials. In fact, for operation at temperatures above 800 °C the only oxides that fit these criteria are doped rare earth chromites. In particular, compositions of the system (La,Sr,Ca)(Cr,Mg)O_3 are the leading interconnect materials. However, compositions of the (Y,Ca)CrO_3 system also have acceptable properties. Rare earth chromites satisfy most requirements but present problems in manufacturing and have a high cost.

6.1. Coefficient of thermal expansion (CTE)

The thermal expansion mismatch of adjacent components in the SOFC stack leads to thermal stress (σ), which can be estimated by: $\sigma=E\Delta a\Delta T$, where E is the elastic (Young) modulus of the interconnect; $\Delta\alpha$ is the difference in CTE between the interconnect and its adjacent component; and ΔT is the change in temperature experienced by this assembly. To minimise the thermal stress and thus improve the stack's thermomechanical stability it is desirable for the interconnect to have a CTE matching that of the positive cathode-electrolyte-negative anode (PEN), which is typically 10.5-12.5$\times10^{-6}$ K^{-1}, and other adjacent components such as seals. Note that the cell structure is often termed the positive-electrolyte-negative (PEN). As a rule of thumb, fcc alloys possess a higher CTE, while bcc alloys have a lower CTE. All duplex SS compositions, such as Carpenter 7-Mo and AL 255, display a higher CTE than their pure ferritic counterparts, but lower than the austenitic SSs, which exhibit a CTE of ~16-20$\times10^{-6}$ K^{-1}, from room temperature to 800 ºC (see Table II for 20-400 ºC). In general, bbc ferritic SSs are the most promising interconnect materials for SOFC stacks.

6.2. Oxidation and corrosion resistance

Two main factors have to be considered: (a) the thickness of the oxide scale typically defines the area-specific resistance (ASR) (Ω cm^2) of the interconnect system, and (b) the thickness of the oxide scale determines the amount of metal loss. According to the oxidation theory described in 1933 [35], oxide growth dominated by diffusion follows the well-known parabolic law:

$$\xi^2 = k_p\, t = \left(\frac{k_p}{(\chi\rho)^2}\right) t = \left(\frac{t}{d^2}\right) (k_g^0)\left[\exp^{-\left(\frac{\Delta E_A}{RT}\right)}\right] \qquad (14)$$

where ξ is the oxide scale thickness (μm); k_p and k_g are the rate constants in thickness and weight, respectively (g^2 cm^{-4} s^{-1}), where k_g is used to measure the oxidation rate of alloy compositions; t is the time (s); χ is the weight fraction of oxygen in the oxide, ρ is the density of the oxide (g cm^{-3}); d is the diffusion distance (mm) ($d^2 = Dt$; D is diffusivity of hydrogen (cm^2 s^{-1}) in the material at the tested temperature); ΔE_A is the activation energy (J mol^{-1}) difference for parabolic growth (corrosion rate = $k(t)^{1/2}$); R is the gas constant (8.314 J K^{-1} mol^{-1}); and T is the absolute temperature. In reality, cracking and spalling (exfoliation) are likely to occur during this time, due to weak bonding between the oxide scale and the matrix,

especially if the interconnect experiences thermal cycling. Alumina-forming alloys possess stronger intrinsic adherence between the oxide scale and bulk matrix than chromia formers, and thus demonstrate better spall-off resistance in thermal cycling. On the other hand, the oxidation and corrosion resistance of alloys at the fuel or anode side are also of great importance. Chromia scales on chromia-forming alloys are not completely dense and impervious to carbon or carbon-containing molecules, and in gaseous environments with sufficient high carbon activities the alloys are prone to carburisation after extended exposure. Stainless steel specimens exposed simultaneously to air on one side and fuel on the other side can lead to anomalous oxidation growth on the air side[36].

The resistance loss in the stack is usually measured by the ASR parameter. The contribution from the oxide scale to the overall ASR can be expressed as:

$$ASR = \frac{\xi}{\sigma} = \frac{k_p t^{1/2}}{\sigma_0 \chi \rho} T\left[\exp^{-\left(\frac{\Delta E_A}{RT}\right)}\right] \qquad (15)$$

For example, chromia-forming E-brite (a ferritic SS) has an excellent oxidation resistance with a rate constant of 0.353×10^{-13} g^2 cm^{-4} s^{-1} at 800 ºC. A scale conductivity (σ) of 0.82×10^{-2} S cm^{-1} at 800 ºC yields an estimated ASR of 83×10^{-3} Ω cm^2 after 1000 h of exposure to air on the cathode side[28]. It should be said that the four-pint method was utilised to determine ASR measurements. This technique involves bringing four equally spaced probes into contact with a material of unknown resistance[37].

In general, chromia-forming ferritic stainless steels are among the most promising candidates as interconnect materials, due to their electrically conducting oxide scale, appropriate thermal expansion behaviour and low cost[17].

As mentioned above, alumina formers might also find applications in stack designs in which the interconnect component does not carry electricity or in which the alumina scale can be bypassed by the electrical path. Alumina-forming alloys not only possess much better surface stability in many environments than chromia-forming compositions, but also exhibit higher mechanical strength than other ferritic structures[38].

Aggressive environments vary over a wide range, i.e. (i) the gases oxygen, air, hydrogen, hydrocarbons and mixtures; (ii) the steam used in the reforming process; (iii) carbon deposits from the cracking reaction, coke formation and combustion gases; and (iv) molten salts present in the system. There are all sorts of other factors that affect the corrosiveness of the environment, such as the effects of thermal cycling; fluctuations in environmental chemistry; the effect of periodic shedding of deposits; the effect of an erosive component in the environment; the rate at which the gas approaches equilibrium as it passes through regions of varying temperature. For all of these reasons, detecting corrosion and assessing life time is a big issue.

Considering high temperature corrosion within this context, a couple of effects should be noted. (1) Section reduction due to loss of scale material resulting from the formation of corrosion products; (2) section reduction due to removal of alloy elements or inward diffusion of the coating layer; (3) changes in the CTE matching properties of materials due to the build-up of a low thermal conductivity surface layer; and (4) degradation due to redox cycling conditions.

It is interesting to note that for many situations the steady-state corrosion rate of materials is largely irrelevant. Nevertheless, the materials are selected to have adequate corrosion lifetimes in the operating environment conditions, and a crucial issue is how they will respond to the real conditions they will experience in service.

6.3. Electrical resistivity

To function properly as a bipolar plate, the interconnect should offer a low resistance electrical path in order to minimise electrical losses within the stack. For heat-resistant alloys, the electrical resistance increases with temperature and is the sum of two parts: bulk resistance and scale resistance. The bulk electrical resistance is typically quite low, $60–130\times10^{-6}$ Ω cm at room temperature, and increases only slightly as the temperature rises. Therefore, in the long term the electrical resistance of the oxide scale dominates the electrical behaviour of heat-resistant alloys during SOFC operation.

7. COATINGS

The poisoning effects of volatile chromium species, notably chromium oxyhydroxide ($CrO_2(OH)_2$), on the electrode/electrolyte interfaces causes increases in both diffusion and charge transfer resistance at the interface and drastically deteriorates cell performance[39]. Thus the alloy surface may have to be modified in order to improve its stability. It has been reported that the application of conductive oxide coatings not only decreases the growth rate of Cr_2O_3 scale but also inhibits or even prevents the evaporation of chromium species from the Cr_2O_3 scale, with which the power output degradation rate is controlled to an acceptable level[40]. Ideally the conductive oxide coating should be an electronic conductor with very low ionic conductivity in order to minimise cationic and anionic ion transport through the coating. It is also prefe-

rable for the coating to be dense and chemically compatible with the adjacent materials. For instance, thermal sprayed coatings have led to stable long-term performance lasting for about 12000 h with a cell voltage degradation rate of less than 1 %/1000 h. Furthermore, recent studies show that the electrical conductivity of Cr_2O_3 oxide on ferritic SSs can be improved by dipping with NiO, lanthanum/titanium and magnesium[41].

In the past, high-temperature coatings were selected predominantly after the component design was finalised. Current designs require the substrate (typically a nickel-base superalloy) to have sufficient inherent resistance to degradation mechanisms to prevent catastrophic reductions in service lifetime in the event of coating failure. Since the materials considered for future substrates may possess less inherent environmental resistance at higher temperatures, the importance of coatings to achieve performance will continue to grow. In future SOFC interconnect designs, coatings will be increasingly viewed as an integral portion of the design process to meet the high demands for system performance.

Although many types of high-temperature coatings are currently in use, they generally fall into one of three types: aluminide, chromide, and MCrAlY. The family of coatings that insulate the substrate from the heat of the gas path, thermal barrier coatings (TBCs), is becoming increasingly important as they start to be used for performance benefits. TBCs are ceramic coatings (partially stabilised zirconia) that are applied to an oxidation-resistant bond coat, typically a MCrAlY or aluminide. The main difficulty with TBCs is that the abrupt change in composition and properties at the interface tends to promote ceramic layer spallation.

After a certain operating exposure time it became clear that chromia scales were inappropriate. The primary reason was that above about 850 ºC in high-velocity gas streams the scale was lost as a result of the further oxidation of the chromia to form the volatile species CrO_3. An alternative solution to this is to develop superalloys with a sufficient aluminium content to form a protective alumina (Al_2O_3) scale[42-44]. However, the development of superalloys for higher strength may affect the alloy's ability to form a protective alumina scale.

The solution to this was to use what is called a 'system' approach, in which the strengthening aspects and the oxidation resistance aspects of the alloy design were separated. This was done by developing coatings that were capable of producing a protective outer alumina scale while maintaining good adhesion to the high-strength substrate.

The issues of first cost, lifetime and repairability are of great importance for the components resulting from these developments, and as yet not all of these potential problems have been solved. Furthermore, there is as yet insufficient field experience to identify what the important issues are, and whether any of these are related with high-temperature oxidation and corrosion. It is obvious that the growth of the oxide on what is called the 'bond coat' (this oxide is referred to in this field as the 'thermally grown oxide' (TGO)), is matter of importance, and the adherence between this and the oxide TBC is also an interesting issue.

The TBC is generally porous, and there are good reasons for this. In fact, at high temperatures the TBC may sinter, and this can have adverse effects on the thermal cycling resistance. An issue of interest to this audience is that there have been doubts as to whether the corrodent species responsible for hot corrosion could 'wick down' to the bond coat and threaten the TGO.

The corrosion of SOFC interconnectors is in many ways similar to that of heat exchangers in gasifiers, where the metal temperatures are relatively high and the gas has very low oxygen activity but high carbon and sulphur activities. If anything, the environment is less severe, because the deposits on the metal surface are usually less aggressive. For these situations, given that the specimen material of choice is low alloy ferritic steels, the concept of relatively low-cost coatings has often been proposed: flame spray high aluminium coatings are generally preferred[45].

8. CHARACTERISATION OF THE CERAMIC/INTERCONNECT SYSTEM

Electrochemical impedance spectroscopy (EIS) is a powerful method that allows us to quantify the three parameters defining a corrosion process: (i) the corrosion rate, through the charge transfer resistance (R_{ct}) (Ω cm^2), and using Faraday's law to estimate the penetration of the attack (μm/day); (ii) mass transport processes (diffusion) defined by the parameter: σ_w (Ω cm^2 s$^{-1/2}$); and (iii) electrochemical double layer capacitance at the metal/solution interface (C_{dl}) (F cm^{-2}) [10 and 46-50].

At low temperature the EIS method allows us to characterise a new material for SOFC applications, giving information of the bulk and the grain boundaries. At high temperature, EIS provides information on the triple-phase boundary (TPB) (see Fig. 1), its polarisation resistance (Ω cm^2), and the difference between low and high frequency intercepts on the real axis.

Thermal barrier coatings (TBC) typically consist of YSZ as top coat and a MCrAlY alloy as bond coat. The bond coat between YSZ and the substrate superalloy is designed not only to promote adhesion of the YSZ to the substrate, but also to afford oxidation resistance. Oxidation of the bond coat is a dominant factor leading to the failure of TBCs. As oxidation proceeds,

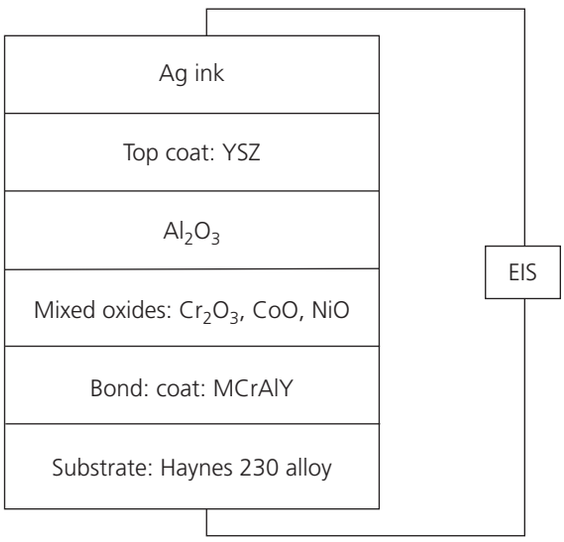

Figure 9. Schema of the oxide layers formed after heating treatment of YSZ/MCrAlY/Haynes 230 alloy system.

Figura 9. Esquema de las capas de óxido formadas después del tratamiento térmico del sistema YSZ/MCrAlY/aleación Haynes 230.

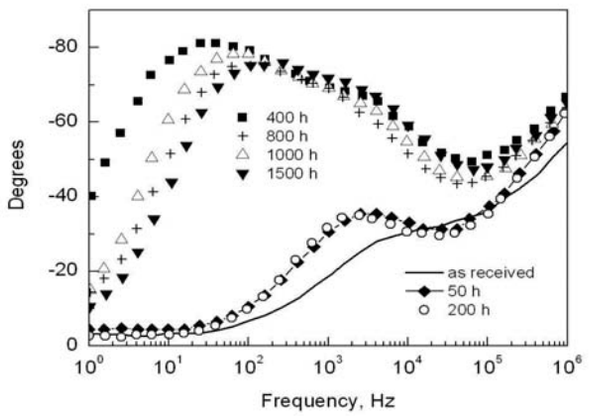

Figure 10. Phase angle versus frequency for YSZ/MCrAlY/Haynes 230 alloy system.

Figura 10. Angulo de fase frente a la frecuencia del sistema YSZ/MCrAlY/aleación Haynes 230.

more and more aluminium element diffuses outward to the bond coat/YSZ interface to form an alumina layer. Characterisation of the alumina layer in TBCs is important in predicting the lifetime of TBCs in service.

The Haynes 230 alloy (a Ni-based superalloy) as substrate (32 wt. % Cr, 14 wt. % W, 2 wt. % Mo, 3 wt. % Fe, 5 wt. % Co, and balance Ni, i.e. ~57 wt. %) with a thickness of 2 mm is sprayed using a HVOF (high-velocity oxygen fuel) MCrAlY (a Co-based superalloy) bond coat (38.5 wt. % Co, 32 wt. % Ni, 21 wt. % Cr, 8 wt. % Al, 0.5 wt. % Y) and a top coat 8 wt. % YSZ. The specimens have been oxidised in a furnace at 1373 K for up to 1500 h. Figure 9 shows a schema, based on SEM observations, of the oxide layers formed after heating treatment[51]. Figure 10 shows a plot of phase angle (θ °) versus frequency (Hz) for the system in figure 9. Three relaxation processes can be observed in the phase angle plot at ~2×10^5 Hz, ~4×10^2 Hz and ~10 Hz. Figure 11 shows the equivalent circuit used to fit impedance data.

The constant phase element (CPE) parameter in figure 11 is a distributed electrical element defined by an empirical function of admittance, given by the following expression:

$$Y = Y_P (j\omega)^{\alpha} \qquad (16)$$

where Y_p is a real frequency-independent constant; j is the imaginary unit: $j^2=(-1)$; and ω is the angular frequency. The α exponent is $0<\alpha<1$ and its physical significance is unclear[52]. On rough surfaces it is referred to as 'capacitance dispersion'. The impedance is not purely capacitive, but has a functional form as if the double-layer capacitance (C_{dl}) were frequency-dependent[53-55]:

$$C_{dl}(\omega) \propto Y_P (j\omega)^{\alpha-1} \qquad (17)$$

When $\alpha=0$ the CPE parameter is a resistor, $R=1/Y_p$; when $\alpha=1$ it is a capacitor, $C=Y_p$; and when $\alpha=(-1)$ it is an inductor, $L=1/Y_p$. Finally, if $\alpha={}^1/_2$, equation (16) can be written as:

$$Y = Y_P (j\omega)^{1/2} \qquad (18)$$

and the CPE is the Warburg admittance[56]. It should be said that different approaches have been made in the literature concerning the conversion of the CPE parameter (Y_p) into a capacitance (C)[57 and 58]:

$$C = Y_P (\omega''_m)^{\alpha-1} \qquad (19)$$

where ω''_m is the angular frequency at which the imaginary part of the impedance (Z") is maximum in a Nyquist plot.

In order to correlate the three relaxation processes defined in figure 10 with the three coating layers of figure 9, the parameter α may be utilised, in spite of the fact that its physical meaning is unclear. For the top coat, the relaxation process is defined at high frequency (~2×10^5 Hz) and the exponent α is basically constant α~0.75, which means that no significant microstructural or compositional change occurred during the oxidation experiment. For the mixed oxides, the relaxation process is defined at intermediate frequency (~4×10^2 Hz) and the α parameter decreased ($0.74<\alpha<0.68$) with increasing oxidation time, which may be interpreted as a decrease in the integrity of the mixed oxides during oxidation. Finally, for the alumina layer the relaxation process is defined at low frequency (~10 Hz) and

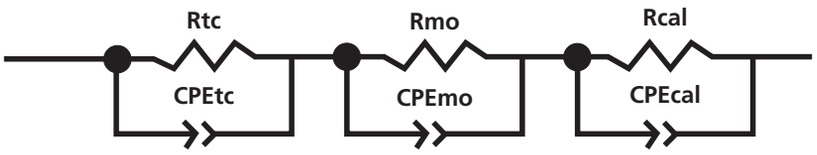

Figure 11. Equivalent circuit used to fit impedance data of figure 10.

Figura 11. Circuito eléctrico equivalente para el ajuste de los datos de impedancia de la figura 10.

the α exponent is close to 1 and nearly constant during the oxidation experiment. Since the substrate and bond coat are highly conductive, the impedance from these elements is negligible. The YSZ/MCrAlY/Haynes 230 alloy system may be described as having a three-layer structure. R_{tc} is the resistance and CPE_{tc} the CPE of the top coat at the interface; R_{mo} is the resistance and CPE_{mo} the CPE of the mixed oxide at the interface; and R_{al} is the resistance and CPE_{al} the CPE of the alumina layer at the interface.

The Sr-doped lanthanum manganite ($La_{0.8}Sr_{0.2}MnO_3$) (LSM)/chromium base alloy (Cr-5Fe-1Y_2O_3) system is manufactured by screen printing and sintering at 1473 K for 2 h in air. The chromium base alloy has a chemical composition of 5 wt. % Fe, 1 wt. % Y_2O_3, and balance Cr, i.e. ~94 wt. %, and a thickness of 1 mm. The LSM powder has been mixed with 50 % solvent terpineol and 50 % ethyl cellulose and screen printed onto the Cr-based alloy foil to form a layer with a thickness of about 70 μm. The specimen was initially dried at 393 K for 6 h in air. Finally, it was heated up to 1473 K in air. Figure 12 shows a schema, based on SEM observations, of the oxide layers formed after heating treatment[7]. The spinel phase $(Mn,Cr)_3O_4$ was present in pores and voids of the LSM layer forming a network surrounding the LSM grains. EIS measurements were performed in the classic two-electrode configuration.

Figure 13 shows a Nyquist plot for the system in figure 12. Two depressed semicircles can be observed which may be attributed to the Cr_2O_3 layer and the $(Mn,Cr)_3O_4$ network. Figure 14 shows the equivalent circuit used to fit impedance data, containing one resistance (R_{LSM}) and two parallel R-CPE in series. Where R_{LSM} is the resistance of the LSM layer, since the Cr-based alloy substrate resistance is negligible, R_1 and R_2 are the resistances and CPE_1 and CPE_2 are the constant phase elements of Cr_2O_3 and $(Mn,Cr)_3O_4$. Due to the porous nature of the $(Mn,Cr)_3O_4$ layer it is reasonable to assume that the exponent α of the CPE for fitting is smaller than that of the Cr_2O_3 layer[59]. The α exponent of the first semicircle (high frequency) is ~0.95 whereas the α value for the second semicircle (low frequency) is ~0.70. Therefore, it is likely that the Cr_2O_3 layer corresponds to the first semicircle whereas the $(Mn,Cr)_3O_4$ phase corresponds to the second semicircle. It is concluded that the LSM/Cr-5Fe-1Y_2O_3 alloy system may be described as having a two-layer structure[32].

Figure 15 shows a Nyquist plot for the LSM/Fecralloy system manufactured at 1473 K for 2 h in air. Only one semicircle can be observed. Since the LSM layer and Fecralloy alloy substrate (22 wt. % Cr, 4.8 wt. % Al, 0.3 wt. % Si, 0.3 wt. % Y, and balance Fe, i.e. ~72.6

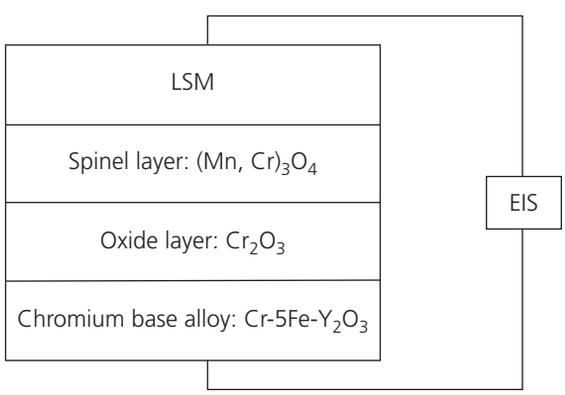

Figure 12. Schema of the oxide layers formed after heating treatment of LSM/chromium base alloy system.

Figura 12. Esquema de las capas de óxido formadas después del tratamiento térmico del sistema LSM/aleación base cromo.

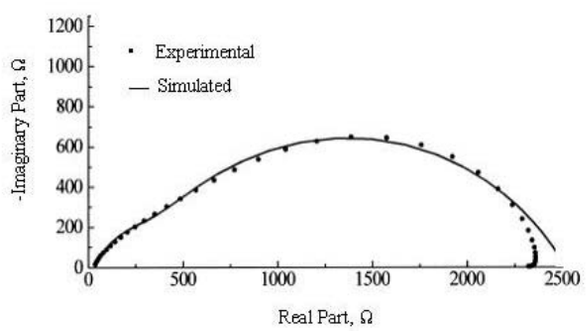

Figure 13. Nyquist plot for LSM/chromium base alloy.

Figura 13. Diagrama de Nyquist del sistema LSM/aleación base cromo.

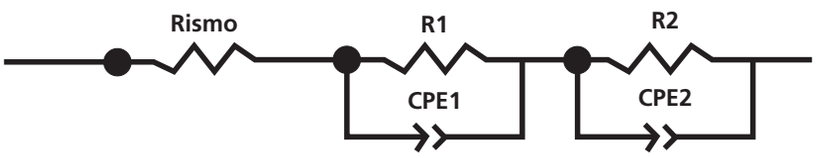

Figure 14. Equivalent circuit used to fit impedance data of figure 13.

Figura 14. Circuito eléctrico equivalente para el ajuste de los datos de impedancia de la figura 13.

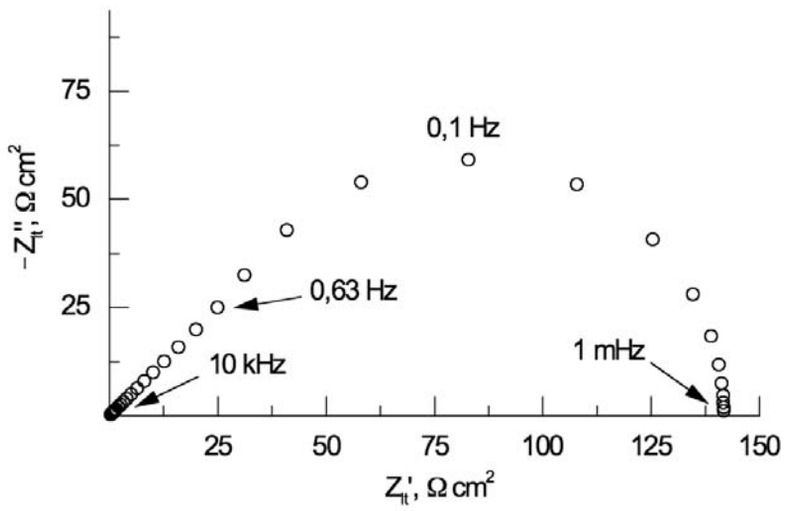

Figure 15. Nyquist plot for LSM/Fecralloy system.

Figura 15. Diagrama de Nyquist del sistema LSM/Fecralloy.

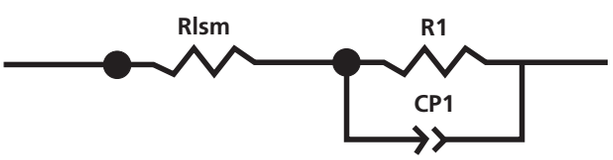

Figure 16. Equivalent circuit used to fit impedance data of figure 15.

Figura 16. Circuito eléctrico equivalente para el ajuste de los datos de impedancia de la figura 15.

wt. %) are electric conductors, the semicircle may be attributed to the oxide layer formed at the interface in the specimen. Figure 16 shows the equivalent circuit used to fit impedance data, containing one resistance (R_{lsm}) and one parallel R_1-C_1 in series. Where R_{lsm} is the resistance of the LSM layer, R_1 and C_1 are the resistance and capacitance of the oxide layer.

8.1. Empirical functions

In order to interpret the depressed semicircles in figures 10, 13 and 15, empirical functions can be used. The most frequently used are discussed in the following paragraph.

(a) Cole-Cole (CC) [60]:

$$Z_{CC} = \frac{R_p}{1 + (j\omega R_p C_{dl})^{\alpha}} \qquad (20)$$

where $0<\alpha<1$.

(b) Davidson-Cole (DC) [61]:

$$Z_{DC} = \frac{R_p}{(1 + j\omega R_p C_{dl})^{\beta}} \qquad (21)$$

where $0<\beta<1$.

(c) Havriliak-Negami (HN) [62]:

$$Z_{HN} = \frac{R_p}{[1 + (j\omega R_p C_{dl})^{\alpha}]^{\beta}} \quad (21)$$

where $0<\alpha<1$ and $0<\beta<1$.

(d) Gerischer (GR) [63-66]:

$$Z_{GR} = Z_0(K + j\omega)^{-1/2} \quad (23)$$

where k is the transfer rate (s^{-1}) of the chemical reaction. Gerischer impedance has been associated to the 'non-faradaic' electrolyte resistance, for thick electrodes. It could be modelled quite reasonably by a 'fractal' modification of the Gerischer expression, i.e. 'single fractal' Gerischer expression ($Z_{GR(s,fr)}$):

$$Z_{GR(s,fr)} = Z_0(K + j\omega)^{-\alpha} \quad (24)$$

The standard Gerischer element (i.e. $(Z_0)^{-1}$) with $\alpha=1/2$, can be modelled by a transmission line model with a 'leaky' capacitance, i.e.:

$$Z_{GR}(\omega) = \left(\frac{r_{cl}}{C_{TPB}}\right)^{1/2}\left[\left(\frac{1}{R_{ct}C_{TPB}}\right) + j\omega\right]^{-1/2} \quad (25)$$

where r_{cl} is the electronic spreading resistance of the electrode; R_{ct} is the charge transfer resistance; and C_{TPB} is the electrochemical capacitance at the triple-phase boundary (TPB).

Much improved modelling of the low frequency end of the data could be obtained through the use of a 'double fractal' Gerischer expression ($Z_{GR(d,fr)}$):

$$Z_{GR(s,fr)} = Z_0[k + (j\omega)^{\beta}]^{-\alpha} \quad (26)$$

where β is less than one (this dispersion relation has the same form as the Havriliak-Negami (HN) dielectric dispersion relation, see equation (22).

9. SUMMARY AND CONCLUSIONS

There are three different important issues to be considered. The interconnector materials are selected on the basis of criteria in which oxidation and corrosion resistance are of major importance. Moreover, it is desirable to improve thermal barrier coatings and protective layers against corrosion. In this way, the selection and design of materials plays a crucial role for the efficiency of the SOFC interconnectors and their lifetime. The approaches to these issues can be described as follows: (i) alloy materials and manufacturing development, (ii) system designs, mainly coating development for corrosion-resistant layers or by the use of thermally-insulating layers, TBC.

For very high-performance SOFC systems, a very highly efficient interconnector is required to minimise electrical losses and to improve the lifetime of the whole SOFC stack system. Therefore, high temperature corrosion behaviour is one of the most important issues to be considered in the SOFC research field.

In general, impedance results allow us to determine the parameters defining the corrosion process. The plots reflected a high frequency part attributed to the bulk resistance of the oxide scale and a low frequency part with higher capacitance attributed to grain boundary or electrode contact impedance. For systems defining three relaxation processes, impedance data was fitted using three parallel resistances-constant phase elements in series for the top coat oxide, mixed oxide, and oxide layer bonded to the substrate material. Finally, for a system defining only one semicircle, the resistance and capacitance allow us to characterise its corrosion behaviour.

Overall, the high operating temperatures of SOFCs can give rise to considerable materials issues like material incompatibilities and instability (thermal and chemical), as well as corrosion and degradation phenomena. Prospective efforts within research and development have been targeted on technologically and cost-effectively optimising materials issues in SOFC systems for commercial applications. In this way, several designs have emerged as good contenders for SOFC systems. The three main types of designs for SOFC systems are as follows: tubular, bipolar monolithic, and bipolar planar. The bipolar design has a bipolar plate that avoids contact between reactant gases placed separately in adjacent cells, preventing them from mixing, and enables the cells to be electrically interconnected. The individual cells are stacked together by means of interconnectors. Concerning impurity tolerance, SOFC systems provide a better allowance because of their high operating temperatures. Current research is being focused on intermediate temperature SOFC systems operating at temperatures in the 550-800°C range. Operating temperature reduction is shown to be highly cost-effective and to reduce materials degradation. Intermediate operating temperatures provide stability amelioration including: better thermal compatibility between different materials, reduced cracking when operating with hydrocarbon fuels, improved material issues such as less thermal stress and more material flexibility, lower heat loss, and minimised corrosion and degradation processes. A priority area is for metallic interconnectors to be developed on SOFC systems operating at intermediate temperature.

Acknowledgement

The author expresses his gratitude to the CSIC of Spain for his contract under the I3P Program.

REFERENCES

[1] L.J.M.J. BLOMEN and M.N. MUGERWA (Eds.), *Fuel Cell Systems*, Springer, New York, U.S.A., 1994, p. 163.

[2] B.C.H. STEELE and A. HEINZEL, *Nature* 414 (2001) 345-352.

[3] T. KOMATSU, H. ARAI, R. CHIBA, K. NOZAWA, M. ARAKAWA and K. SATO, *Electrochem. Solid-State Lett.* 9 (2006) A9-A12.

[4] Z.P. SHAO and S.M. HAILE, *Nature* 431 (2004) 170-173.

[5] D.M. BASTIDAS, S. TAO and J.T.S. IRVINE, *J. Mater. Chem.* 16 (2006) 1603-1605.

[6] J.C. RUÍZ-MORALES, J. CANALES-VÁZQUEZ, C. SAVANIU, D. MARRERO-LÓPEZ, W. ZHOU and J.T.S. IRVINE, *Nature* 439 (2006) 568-571.

[7] J.Q. LI and P. XIAO, *J. Eur. Cram. Soc.* 21 (2001) 659-668.

[8] S.P. JIANG and S.H. CHAN, *J. Mater. Sci.* 39 (2004) 4405-4439.

[9] C.M. CHUN and J.D. MUMFORD, *J. Electrochem. Soc.* 147 (2000) 3680-3686.

[10] S.B. ADLER, *Solid State Ionic.* 135 (2000) 603-612.

[11] S.B. ADLER, J.A. LANE and B.C.H. STEELE, *J. Electrochem. Soc.* 143 (1996) 3554-3564.

[12] Y. MATSUZAKI and I. YASUDA, *Solid State Ionics* 132 (2000) 261-269.

[13] R.J. GORTE, S. PARK, J.M. VOHS and C. WANG, *Adv. Mater.* 12 (2000) 1465-1469.

[14] J.T.S. IRVINE, F.G. JONES and P.A. CONNOR, International Patent Application, PC/GB2002/ 004726.

[15] J.T.S. IRVINE and S. TAO, British Patent Application, 2002, 0217794.79020115.3.

[16] S. LINDEROTH, P.V. HENDRIKSEN, M. MOGENSEN and N. LANGVAD, *J. Mater. Sci.* 31 (1998) 5077-5082.

[17] Z. YANG, M.S. WALKER, P. SINGH, J.W. STEVENSON and T. NORBY, *J. Electrochem. Soc.* 151 (2004) B669-B678.

[18] N.Q. MINH, *J. Am. Ceram. Soc.* 76 (1993) 563-588.

[19] N.Q. MINH, *Solid Sate Ionics* 174 (2004) 271-277.

[20] S.C. SINGHAL, *Solid State Ionics* 135 (2000) 305-313.

[21] S. TAO and J.T.S. IRVINE, *Nat. Mater.* 2 (2003) 320-323.

[22] M.L. PERRY and T.F. FULLER, *J. Electrochem. Soc.* 149 (2002) S59-S67.

[23] W.J. QUADAKKERS, H. GREINER and W. KOCK, *Proceedings of the 1st European SOFC Forum*, U Bossel (Ed.), Switzerland, (1994), p. 525.

[24] J.M. BASTIDAS, J.L. POLO, C.L. TORRES and E. CANO, *Corros. Sci.* 43 (2001) 269-281.

[25] J.M. BASTIDAS, C.L. TORRES, E. CANO and J.L. POLO, *Corros. Sci.* 44 (2002) 625-633.

[26] J.M. RUÍZ-ROMERO, F. CORPAS, F.J. IGLESIAS, L.E.G. CAMBRONERO and J.M. RUÍZ-PRIETO, *Rev. Metal. Madrid* Vol. Ext. (2005) 269-271.

[27] L. NARVÁEZ, E. CANO, D.M. BASTIDAS and P.P. GÓMEZ, *Rev. Metal. Madrid* Vol. Ext. (2005) 160-164.

[28] Z. YANG, K.S. WELL, D.M. PAXTON and J.W. STEVENSON, *J. Electrochem. Soc.* 150 (2003) A1188-A1201.

[29] W.J. QUADAKKERS, V. SHEMET, D. SEBOLD, R. ANTON, E. WESSEL and L. SINGHEISER, *Surf. Coat. Tech.* 199 (2005) 77-82.

[30] J.L. POLO, E. CANO, D.Y. KONG and J.M. BASTIDAS, *Corrosion* 58 (2002) 670-674.

[31] V. KOCHUBEY, H. AL-BADAIRY, G. TATLOCK, J. LEGOZE, D. NAUMENKO and W.J. QUADAKKERS, *Mater. Corros.* 56 (2005) 848-853.

[32] N.Q. MINH and T. TAKAHASHI, : *Science and Technology of Ceramic Fuel Cells*, Elsevier, Amsterdam, (1995), p. 230.

[33] M. GONZÁLEZ-CUENCA, W. ZIPPRICH, B.A. BOUKAMP, G. PUDMICH and F. TIETZ, *Fuel Cells* 1 (2001) 256-264.

[34] Y. LARRING, R. HAUGSRUD and T. NORBY, *J. Electrochem. Soc.* 150 (2003) B374-B379.

[35] C. WAGNER, *Z. Phys. Chem.* 21 (1933) 25-41.

[36] Z. YANG, M.S. WALKER, P. SINGH and J.W. STEVENSON, *Electrochem. Solid-State Lett.* 6 (2003) B35-B37.

[37] N. BOWLER and Y. HUANG, *Meas. Sci. Technol.* 16 (2005) 2193-2200.

[38] W.A. MEULENBERG, O. TELLER, U. FLESCH, H.P. BUCHKREMER and D. STEVER, *J. Mater. Sci.* 36 (2001) 3189-3195.

[39] Y. MATSUZAKI and I. YASUDA, *J. Electrochem. Soc.* 148 (2001) A126-A131.

[40] K. HILPERT, D. DAS, M. MILLER, D.H. PECK and R. WEISS, *J. Electrochem. Soc.* 143 (1996) 3642-3647.

[41] V.A.C. HAANAPPEL, V. SHEMET, I.C. VINKE, M. GROSS, T. KOPPITZ, N.H. MENZLER, M. ZAHID and W.J. QUADAKKERS, *J. Mater. Sci.* 40 (2005) 1583-1592.

[42] W.R. OSORIO, C.M.A. FREIRE and A. GRACIA, *Rev. Metal. Madrid* Vol. Ext. (2005) 160-164.

[43] J.A. PICAS, A. FORN, R. RILLA and E. MARTIN, *Rev. Metal. Madrid* Vol. Ext. (2005) 197-201.

[44] D.G. MORRIS and M.A. MUÑOZ-MORRIS, *Rev. Metal. Madrid* Vol. Ext. (2005) 498-501.

[45] *Fuel Cell Handbook*, 5th Edition, EG&G Services, Parsons, Inc. and Science Applications International Corporation, US Department of Energy, Morgantown, West Virginia, (2002).

[46] J.E. BAUERLE, *J. Phys. Chem. Solids* 30 (1969) 2657-2670.

[47] T. VAN DIJK and A.J. BURGGRAAF, *Phys. Stat. Sol.* 63 (1981) 229-240.

[48] E.J.L. SCHOULER, N. MESBAHI and G. VITTER, *Solid State Ionics* 9 (1983) 989-996.

[49] S.B. ADLER, J.A. LANE and B.C.H. STEELE, *J. Electrochem. Soc.* 144 (1997) 1881-1890.

[50] J. AGRISUELAS, J.J. GARCÍA-JAREÑO, J. GREGORI, D. GIMÉNEZ-ROMERO, R. GONZÁLEZ, M.P. PEÑA and F. VICENTE, *Rev. Metal. Madrid* Vol. Ext. (2005) 265-268.

[51] X. WANG, J. MEI and P. XIAO, *J. Eur. Ceram. Soc.* 21 (2001) 855-859.

[52] U. RAMMELT and G. REINHARD, *Electrochim. Acta* 35 (1990) 1045-1049.

[53] Z. KERNER and T. PAJKOSSY, *Electrochim. Acta* 46 (2000) 207-211.

[54] O. COMINELI, H. LUO, H.M. LIIMATAINEN and L.P. KARJALAINEN, *Rev. Metal. Madrid* Vol. Ext. (2005) 407-411.

[55] E. PEÓN, A. JIMENEZ-MORALES, E. FERNÁNDEZ-ESCALANTE, M.C. GARCIÁ-ALONSO, M.L. ESCUDERO and J.C. GALVÁN, *Rev. Metal. Madrid* Vol. Ext. (2005) 479-482.

[56] M. CAI and S.-M. PARK, *J. Electrochem. Soc.* 143 (1996) 3895-3902.

[57] G.O. ILEVBARE and J.R. SCULLY, *Corrosion* 57 (2001) 134-152.

[58] C.H. HSU and F. MANSFELD, *Corrosion* 57 (2001) 747-748.

[59] M. KUPEZYK and W. MISTAK, *Rev. Metal. Madrid* Vol. Ext. (2005) 483-487.

[60] K.S. COLE and R.H. COLE, *J. Chem. Phys.* 10 (1942) 98-105.

[61] D.W. DAVIDSON and R.H. COLE, *J. Chem. Phys.* 19 (1951) 1484-1490.

[62] S. HAVRILIAK and S. NEGAMI, *Polymers* 8 (1967) 161-210.

[63] M. SLUYTERS-REHBACH and J.H. SLUYTERS, : *Comprehensive Treatise of Electrochemistry*, E. Yeager, J.O'M. Bockris, B.E. Conway, S. Sarangapani, (Eds.), Vol. 9, Plenum Press, New York, (1984), p. 274.

[64] S.B. ADLER, *Solid State Ionic.* 111 (1998) 115-124.

[65] E. BARSOUKOV and J.R. MACDONALD, : *Impedance Spectroscopy Theory, Experimental, and Applications*, 2nd Ed. Wiley-Interscience, Hoboken, New Jersey, (2005), p. 54.

[66] J.L. POLO, E. CANO and J.M. BASTIDAS, *J. Electroanal. Chem.* 537 (2002) 183-187.